PILOT STUDY ON THE FEASIBILITY OF REPLACING INVASIVE HEART PRESSURE MEASUREMENTS WITH NON-INVASIVE MAGNETIC RESONANCE ELASTOGRAPHY AS A WAY TO REDUCE RODENT NUMBERS IN PRE-CLINICAL RESEARCH

by

Neuza Filipa Botelho da Silva

March 2013

PILOT STUDY ON THE FEASIBILITY OF REPLACING INVASIVE HEART PRESSURE MEASUREMENTS WITH NON-INVASIVE MAGNETIC RESONANCE ELASTOGRAPHY AS A WAY TO REDUCE RODENT NUMBERS IN PRE-CLINICAL RESEARCH

Estudo Piloto da Viabilidade de Substituição das Medições Invasivas de Pressão do Coração pelo Método Não-invasivo Elastografia por Ressonância Magnética como Forma de Redução do Número de Roedores na Pesquisa Pré-clínica

Thesis presented to Escola Superior de Biotecnologia of the Universidade Católica Portuguesa to fulfil the requirements of Master of Science degree in Biomedical Engineering

by

Neuza Filipa Botelho da Silva

Place: British Heart Foundation Experimental MR Unit, Wellcome Trust Centre for Human Genetics, University of Oxford, Oxford, United Kingdom.

Supervision: Doctor Jurgen Schneider
Co-Supervision: Doctor Mahon Maguire

March 2013

Resumo

Background: Imagem e Espectroscopia por Ressonância Magnética são técnicas fenotípicas que permitem a caracterização não-invasiva da função cardíaca em roedores. No entanto, ao avaliar a função miocárdica, as fases do ciclo cardíaco onde ocorrem as taxas máximas de geração de pressão e relaxamento não são directamente acessíveis com técnicas de imagem. Esta informação está apenas disponível recorrendo a cateterismo, sendo que se trata de um procedimento invasivo e terminal em roedores. A Elastografia por Ressonância Magnética mensura a deformação de um tecido após a estimulação mecânica e tem o potencial de aceder de forma não-invasiva à pressão ventricular *in vivo*, como foi demonstrado com sucesso em porcos e corações humanos. Este projecto tem como objectivo a construção de um sistema que permite a excitação mecânica no interior do magnete com a adequada amplitude e gama de frequência, necessárias para experiências murinas.

Metodologia: Foi necessário o desenvolvimento do *hardware* de Elastografia necessário à estimulação mecânica de tecidos, compatível com o sistema existente de manipulação dos animais. Sequências de Ressonância Magnética foram ainda implementadas e equipadas com um gradiente de sensibilização de movimento por forma a codificar a deformação das ondas de cisalhamento. O sistema de Elastografia bem como as sequências formam testados em géis de agarose com uma gama de frequências até aos 1,5 kHz de vibração, essenciais para dimensões do coração de ratos. Posteriormente, um gel de dois compartimentos com diferentes concentrações de agarose foi excitado utilizando a configuração de Elastografia. Finalmente, um rato morto foi submetido a exames de Elastografia por Ressonância Magnética.

Resultados: Houve uma clara e uniforme penetração das ondas de cisalhamento nas experiências com géis de agarose. Todos os espectros mostraram um padrão de deslocamento de fase em toda a amostra, o que correspondeu à propagação das vibrações mecânicas. O gel de 0,5% de agarose deformou mais do que o gel de 1%, resultando num comprimento de onda mais curto que o comprimento de onda encontrado no gel mais rígido. Os resultados também mostram maior atenuação das ondas no gel de 1%, quer a 500 Hz quer a 1000 Hz de frequência de vibração, quando comparado com a propagação de ondas no gel de 0,5%. Na amostra de dois compartimentos, observou-se que as ondas penetraram não-uniformemente os dois compartimentos. Houve uma melhor propagação das ondas no gel de 0,5% de agarose do que no gel de 2%, resultando num comprimento de onda mais curto no gel menos rígido. No gel com maior rigidez não foi observável uma onda inteira numa única imagem, enquanto que no gel mais *soft* são observados seis ciclos completos de vibração. Nas experiências com o rato, verificou-se uma forte distinção dos tecidos aquando da passagem das vibrações. Os tecidos deformaram-se em função da sua rigidez que se traduziu em diferentes variações de fase no fígado e no coração.

Conclusões: Neste projecto foi concebível um sistema bem-sucedido de estimulação mecânica dos tecidos. Foi qualitativamente demonstrado que a aplicação de excitação mecânica por ondas de cisalhamento pode ser um método para codificar propriedades mecânicas de um objecto heterogéneo. Assim, este projecto representou um enorme passo no desenvolvimento de uma técnica capaz de fazer medições de pressão ventricular em ratos.

Abstract

Background: Magnetic Resonance Imaging (MRI) and Spectroscopy (MRS) are phenotyping techniques that allow for a non-invasive characterization of cardiac function in rodents. However, when assessing myocardial function, the isovolumic phases of the cardiac cycle are not directly accessible to imaging techniques, yet this is where maximal rates of pressure generation and relaxation occur. This type of information is only available using LV catheterization, which in rodents is an invasive and terminal procedure, requiring new experimental groups every time-point. Magnetic Resonance Elastography (MRE) measures shear deformation following mechanical tissue stimulation and has the potential to non-invasively access ventricular pressure in vivo, as successfully demonstrated in pig and human hearts. Therefore, this project aims to build a setup, which allows for mechanical stimulations inside the magnet with the appropriate amplitude and frequency range required for murine experiments.

Methodology: Core to this project was the development of the MRE hardware required for the mechanical tissue stimulation and compatible with the existing animal handling system. MRI sequences needed to be implemented to equip them with motion-sensitizing gradient to encode shear deformation. In order to validate the MRE setup and the MRI sequences, phantoms of different concentrations of agarose were excited over a wide range of frequencies. The frequencies ranged from hundreds of Hz up to 1.5 kHz. MRE experiments were subsequently performed on a two-compartment phantom with different concentrations of agarose. Finally, a dead mouse was subjected to MRE examinations.

Results: There was a clear uniform penetration of shear waves in phantom experiments. All phantoms demonstrated a pattern of phase shifts across the sample, which corresponded to propagation of mechanical vibrations. The gel of 0.5% agarose deformed more than the 1% agarose gel, resulting in a wavelength shorter than the wavelength found in stiffer gel. The results also show higher attenuation of shear waves in 1% agarose gel, either at 500 Hz or 1000 Hz of vibration frequency, when compared with the propagation of waves in 0.5% agarose gel. In the two-compartment phantom, shear waves penetrated non-uniformly the phantom. There was a better propagation of waves in the 0.5% gel than in the 2% one, resulting in a shorter wavelength in the softer gel than the rigid one. In the gel with higher level of stiffness the wavelength exceeded the dimensions of the gel while in the softer gel were observed six complete vibration cycles. In the mouse experiments, there was a strong tissue distinction when vibrations passed through them. The tissues deformed depending on their rigidity which translated into different spins phase variations either in the liver or in the heart.

Conclusions: A setup to provide tissue mechanical stimulation in a small bore pre-clinical MR system was successfully developed. It was qualitatively demonstrated that the application of shear wave mechanical excitation may be a method to encode mechanical properties of a heterogeneous object. Thus, this project represented a major step in the ability to develop a technique for indirect LV pressure measurements in mice.

Acknowledgements

I am extremely grateful to Dr Jurgen Schneider for supervising me during the development of this project and for all the knowledge transmitted. I would like to express my sincerest gratitude for having given me the incredible opportunity to do my Master Thesis at the University of Oxford and for having integrated me in the BMRU group.

I am very thankful to Dr Mahon Maguire for all the knowledge, sound advice and valuable help, throughout the semester.

I would like to enlarge my thanks to Mrs. Lee-Anne Stork, Ms. Vicky Thornton, Dr Kiterie Faller, Mr. Kyle Caldock, Dr Maélène Lohezic and Dr Irvin Teh for having welcomed me so kindly in the BMRU group.

I acknowledge, in a very particular way, the support of Professor João Paulo Ferreira over these months. I appreciated all the efforts to make this experience possible.

I would like to thank my family for all the love and motivation.

Lastly, an enormous and special thank you to José Santos for all encouragement, precious care and unconditional support, along this journey.

Table of Contents

Page

List of Figures

Page

List of Abreviations

FD	Frequency Domain
FT	Fourier Transformation
FID	Free Induction Decay
FOV	Field of View
B_0	Static Magnetic Field
BMRU	British Heart Foundation Experimental Magnetic Resonance Unit
G_{PE}	Phase-encoding Gradient
G_{RO}	Read-out Gradient
G_{SS}	Slice-selection Gradient
i	Sinusoidal current
LV	Left-ventricular
M	Macroscopic Magnetization
M_{xy}	Transverse Magnetization
M_z	Longitudinal Magnetization
MRI	Magnetic Resonance Imaging
MRS	Magnetic Resonance Spectroscopy
NMR	Nuclear Magnetic Resonance
PE	Phase-encoding
P-V	Pressure-Volume
RF	Radiofrequency
RO	Read-out
ROI	Region of Interest
SS	Slice-selection
S-V	Stiffness-Volume
T_1	Spin-lattice Relaxation Time
T_2	Spin-spin Relaxation Time
TD	Time Domain
TE	Echo Time
TR	Repetition Time
US	Ultrasound
V_{pp}	Volts Peak to Peak
WAV	Wave Amplitude Variation

CHAPTER 1

Introduction

1.1 Background and Importance

Many research centers around the world are arduous and continuously trying to deepen their knowledge about the heart of rodents, including its function, anatomy, structure and metabolism. Mice have been intensely studied due to its well-characterized genome and its similarity with human genome, as well as the ability to alter specific genes and their products (Field, 1993). Magnetic Resonance Imaging (MRI) and Spectroscopy (MRS) are the most sophisticated phenotyping techniques that allow for a non-invasive quantification of cardiac function of mouse models *in vivo*. Particularly, high-resolution magnetic resonance cine imaging (cine-MRI) has been applied successfully to quantify myocardial mass and left-ventricular function in mice (Ruff *et al*., 1998; Schneider *et al*., 2003; Schneider *et al*., 2008). By a way of example, Dall'Armellina *et al*. (2012) presented an optimized method based on phase-contrast MRI that allows for a comprehensive assessment of regional cardiac function in mouse, through the measurement of murine transmural wall motion.

However, important functional characteristics of the cardiac cycle, i.e. the alteration of ventricular pressure during the isovolumic phase, are not directly accessible to MRI. The isovolumic phases of the cardiac cycle reflect myocardial contractility and relaxation, which is where the maximum rates of pressure take place (Elgeti *et al*., 2009). The pressure-volume (P-V) relationship is a highly reliable parameter for assessing myocardial contractility and the determination of this relationship requires the simultaneous acquisition of ventricular volume and pressure data (Elgeti *et al*., 2008). This type of information is only available using LV catheterization, which typically involves cannulation of the right carotid artery and advancing a microtipped cannula retrograde into the left ventricle. This procedure is not only technically very challenging, but is also terminal for mice. Furthermore, especially in small animal models with total blood volume of a few millilitres, the smallest blood loss would lead to a pressure hemodynamic changes that may affect cardiac results significantly.

Magnetic Resonance Elastography (MRE) is a promising technique to potentially overcome this limitation and non-invasively access to ventricular pressure *in vivo*, as it has been shown that changes in myocardial stiffness are directed correlated to the change in intraventricular pressure (Sack *et al*., 2009).

MRE makes use of external mechanical stimulation to encode mechanical properties of the tissues by visualizing and measuring the oscillating shear displacements (Parker *et al*., 1990; Muthupillai *et al*., 1995).

To date, this method has only been applied to hearts of pigs (Elgeti *et al*., 2009; Kolipaka *et*

al., 2010; Xu *et al*., 2011) and humans (Elgeti *et al*., 2008; Sack *et al*., 2009; Elgeti *et al*., 2010a; Elgeti *et al*., 2010b; Elgeti *et al*., 2012; Tzschatzsch *et al*., 2012) as a way to access to ventricular pressure measurements *in vivo*. The MRE for small animals (μMRE) also has been a tool to determine viscoelastic parameters of rat liver (Salameh *et al*., 2009) and kidney (Shah *et al*., 2004), as well as mouse brains (Atay *et al*., 2008), but not yet to mouse hearts.

Having a technique capable to non-invasively access LV pressure not only represent a valuable tool for scientists studying progression and treatment of heart disease, but also allow for a longitudinal investigation in the same animal, leading to a reduction of animal numbers required in cardiovascular research. The MRE technique would thus hold a tremendous advantage to determine relationships between tissues viscoelastic behavior and cardiac function, as a way to reduce rodent numbers in pre-clinical research.

1.2 Nuclear Magnetic Resonance

Nuclear Magnetic Resonance is a non-invasive technique that is being widely used to study living tissue. It is particularly suitable for the heart as it is able to obtain diagnostic images and to provide a great deal of physiological information (Myerson *et al*., 2011).

The principles of NMR are well described in the literature. Thus, in this section is briefly summarized only the basis of NMR following the papers by Fullerton (1982), Karstaedt *et al*. (1983), Gadian (1995) and Graaf (2007).

1.2.1 Nuclei and Magnetic Field

NMR utilizes the magnetic properties of certain atomic nuclei and its interaction with static magnetic field B_0 to generate the NMR signal. MRI typically uses the signal of protons contained in tissue to create high detailed images of the human body. Although many nuclei possess a magnetic moment necessary for NMR, the hydrogen has the highest sensitivity and abundance in the human body required to generate high-resolution MR images.

The phenomena of NMR can be classically described as a precession of nucleus around its own axis, resulting in an angular momentum. Their spinning produces a magnetic moment as the spins act as small magnetic bars. The spins are randomly oriented in the absence of an external magnetic field. However, when placed in a static magnetic field B_0, the nuclei align along the direction of the external field, with parallel and antiparallel orientations, corresponding to low and high energy levels, respectively. The state with lower energy has a slightly higher density population than the higher energy level. The magnetic field exerts a torque on the magnetic moment causing the precession of the magnetic moments of nuclei about the external magnetic field with an angular frequency, called Larmor Frequency, proportional to the magnetic field. The alignment of individual magnetic moments with the axis of external the field (z-axis) generates a macroscopically measurable net magnetization.

1.2.2 The NMR signal

The resonance phenomenon occurs when a radiofrequency (RF) electromagnetic field is applied perpendicular to the static magnetic field B_0. This oscillating magnetic field, in the form of radio waves, rotates synchronously (in resonance) with the precessing spins and perturbs the spins away from their state of equilibrium. After a RF pulse is applied, the resulting signal, which is called free induction decay (FID), is collected. The FID presents a damped sinusoidal shape, which is a time domain (TD) signal. This signal is converted to a frequency domain (FD) to decode spatial information. This conversion is made using the mathematical operation, called Fourier Transformation (FT).

Two main commonly used pulse sequences in MRI are the spin-echo and the gradient-echo. In the spin-echo sequence, an 180º RF pulse is applied a few milliseconds after an initial 90º pulse, to generate an echo that is collected at a specific TE (echo time). Conversely, the gradient-echo sequence results from applying a dephasing gradient after excitation of RF pulse. Upon reversal of

this gradient, the magnetization gradually rephrases to produce a gradient echo. Either sequence is repeated at intervals TR (repetition time).

1.2.3 Relaxation Times

Following the perturbation of radiofrequency field, the magnetization returns to its initial equilibrium configuration by a process called relaxation. This process is characterized by two time constants T_1 and T_2, i.e. spin-lattice relaxation time and spin-spin relaxation time, respectively. The spin-lattice relaxation time, also called *longitudinal relaxation time*, is the time for perturbed magnetization to along the z axis, i.e. in direction of applied magnetic field B_0.

On the other hand, the spin-spin relaxation time, or *transverse relaxation time*, describes the decay of the transverse x-y component of the magnetization, perpendicularly to the B_0. Thus, in-phase spins precess at slightly different frequencies with a certain diphase with respect to another. This relaxation time is due to intrinsic interactions among the nuclei themselves.

1.2.4 MR Imaging

MRI makes use of spatially encoded frequency and phase to form an image.

The precession frequency of nuclei spins is proportional to the local magnetic field strength. Thus, changing linearly the magnetic field strength along a particular axis, it results in resonance frequency changes in each position. Through the employment of magnetic field gradients along the axis, MRI is able to provide localized information of the signal.

Three gradients are exploited in MRI to encode position and form the image, namely slice-selection (G_{SS}), phase-encoding (G_{PE}) and read-out (G_{RO}) (also known as frequency-encoding) gradients. To select a slice of interest, a gradient is applied and the magnetic field experienced by the nuclei varies linearly along z-axis. Therefore, the nuclei will precess with a slightly different frequency at each position. A frequency-selective RF pulse will thus only excite a selected slice of tissue. Further, the second step in spatial encoding consists in applying a phase-encoding gradient. Such gradient modifies the spin resonance frequencies and induces a phase depending on the position. Rephrasing this experiment N-times with phase-encoding gradients of different strengths will induce phase changes dependent on the position of the spins. Lastly, the encoding in the 3rd dimension is achieved by means of a frequency-encoding gradient, applied simultaneously during receiving the signal. It, also called as read-out gradient, produces a magnetic gradient field present during the MR signal acquisition to encode signals into different Larmor frequencies, depending on their position within the gradient field.

1.3 Magnetic Resonance Elastography

1.3.1 Elasticity

Many cardiovascular diseases and disorders are associated with hemodynamic dysfunction. The heart's ability to contract and pump blood thought the vascular system primarily depends on the elasticity of the myocardium (Sack *et al*., 2009). The characterization of viscoelastic properties has also been shown as a promising technique and an attractive target for investigators accessing mechanical properties of the soft tissues (Parker *et al*., 1990; Ophir et al., 1991; Muthupillai *et al*., 1995, Muthupillai *et al*., 1996). Pathological changes in the stiffness of biological tissues are generally known to be associated with lesions, such as tumors and other diseases (Strinivasan *et al*., 2004).

MRE has shown a rapid progress in the assessment of the viscoelastic behavior of human organs that are not physically palpable from the body surface. Thus, this technique has been performed in order to evaluate the usefulness of elastography in imaging tissue stiffness. On the other hand, MRE has been shown as a propitious means capable to assess important functional characteristics of the heart, such as myocardial elasticity changes during cardiac cycle. Moreover, it has been demonstrated that myocardial stiffness is directly associated with the change in ventricular pressure (Sack *et al*., 2009; Elgeti *et al*., 2009; Kolipaka *et al*., 2010).

1.3.2 Basis of MRE

MRE is an emerging MRI technique to non-invasively and quantitatively image mechanical properties of soft tissues *in vivo* (Muthupillai *et al*., 1995; Manduca *et al*., 2001; Manduca *et al*., 2003). The basis of MRE is in external mechanical stimuli via vibrations that produce tissue displacements on the order of nanometres or micrometres (Parker *et al*., 1990; Muthupillai *et al*., 1995). The experimental setup allowed micro-meter scale vibrations to be transmitted from the actuator tip along the tissue, by a periodic motion of the actuator.

Studies have been demonstrated that the mechanical vibrations can be generated either acoustically or via a solenoid coil in a magnetic field. In the first instance, the vibrations are transferred to a mechanical actuator which, connected to a loudspeaker, is driven by a sinusoidally alternating current provided by a function-generator-controlled audio amplifier (Klatt *et al*., 2006). The second approach utilizes a sinusoidal current with a frequency of a few tens of Hz to the kHz-range provided by a frequency generator. This current drives a solenoid coil in the magnetic field, resulting in an electromagnetic torque that moves the mechanical actuator (Atay *et al*., 2008).

Propagating shear waves in tissue are encoded into phase accumulation using MRE. The MRI sequence needs to be modified with motion-sensitizing gradients. After continuous harmonic motion is induced in the tissue, the motion-sensitizing gradient oscillates at the same frequency as the applied motion and causes the nuclear spins to accumulate phase, encoding shear deformation. As a result, the phase of the data is proportional to displacement (Sack *et al*., 2009; Mariappan *et al*., 2010; Glaser *et al*., 2012).

Figure 1.1 illustrates the phase accumulation using MRE. The three rows of circles represent three individual spins and the portion filled in represents the phase of a spin at a particular time. The

five columns represent a complete cycle. The amount of phase that a spin accumulates at a given time is directly proportional to the magnetic field strength at that point. Thus at t_2 the upper and lower spins accrue more phase than the middle spin because they have been displaced by vibration into a higher magnetic field. At t_4 the spins are displaced in the opposite direction, however the gradient field has also switched direction and the upper and lower spins again accrue more phase than the middle spin. The net results is an image whose phase is proportional to displacement at a particular time during one cycle (Atay *et al*., 2008).

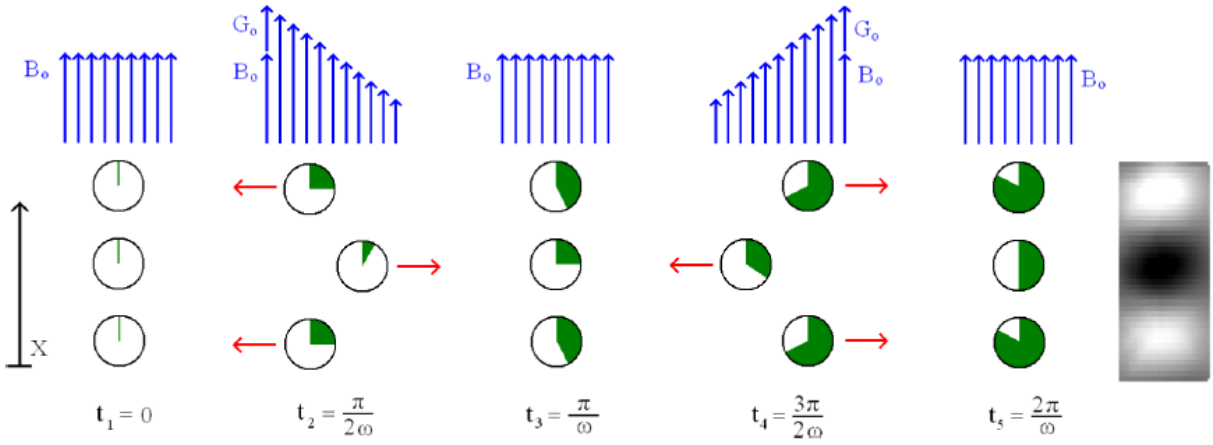

Figure 1.1. Illustration of phase accumulation using MRE. The motion-sensitizing gradients cause the nuclear spins to accumulate phase as they oscillate with the gradients. As a result the phase image of the data exhibits contrast proportional to displacement (Atay *et al*., 2008).

The primary studies addressed the elasticity of tissues as a method to differentiate between normal soft tissue and injured tissues were studies by sonoelasticity (Parker *et al*., 1990). Muthupillai *et al*. (1995) also shown that MRE could measure the wave amplitude variations (WAV) to related that with the tissue dependent shear-elastic and shear-viscous behaviour. Correlations between the modulus images and strain elastograms have been described in the literature in order to relating the change in tissue elasticity as indication of the presence of tumors (Srinivasan *et al*., 2004) or the response to treatments (Techavipoo *et al*., 2004).

1.3.3 Cardiovascular MRE

More recently, cardiovascular MRE has been developed as a fundamental tool practised in the measurements of important parameters in hearts. This method has been described in pig heart (Elgeti *et al*., 2009; Kolipaka *et al*., 2010; Xu *et al*., 2011) as well as in human heart (Elgeti *et al*., 2008; Sack *et al*., 2009; Elgeti *et al*., 2010a; Elgeti *et al*., 2010b; Tzschatzsch *et al*., 2012; Elgeti *et al*., 2012). More specifically, Elgeti *et al*. (2009) have shown that a WAV-MRE is a suitable technique for

non-invasively determining relative changes in left ventricular pressure throughout the cardiac cycle in pig. Wave propagation is dependent on the tissue viscoelastic properties and thus the WAV parameter is highly related with tissue dependent shear-elastic and shear-viscous behaviour. It results from changes in myocardial stiffness during the cardiac cycle. Specifically, they demonstrated a correlation between wave amplitudes and LV pressure and also between wave amplitudes and LV diameter. Similarly, loops of WAV amplitude and LV diameter were constructed. Furthermore, studies with MRI were made to quantify shear stiffness of normal myocardium throughout the cardiac cycle *in vivo* in pig model (Kolipaka *et al*., 2010). They proved that the myocardium stiffness varies between systole and diastole and presented concordant stiffness-volume (S-V) and P-V loops. A linear correlation between shear stiffness and pressure was also shown. On the other hand, Sack *et al*. (2009) proposed non-invasive quantification of elastic ratios of myocardium elasticity for different phases of the cardiac cycle in human heart with MRE. Finally, Elgeti *et al*. (2010) quantified isovolumetric times, namely isovolumetric tension time and isvolumetric elasticity relaxation time, which allied with morphology and elasticity of the heart provided by MRE, symbolized a promising and novel measure of cardiac dynamics.

CHAPTER 2

Methodology

2.1 Hardware Development

The primary aim of this project was the development of a setup to provide mechanical tissue stimulations inside the magnet. The assembly was mounted in a semi-cylindrical plastic mouse cradle with inner diameter of 39 mm, and was based on the design of Atay *et al*. (2008). The mechanical actuator consisted of a small solenoid coil attached to a rod with the coil positioned perpendicularly to the static magnetic field (Figure 2.1). The coil is driven by a sinusoidal current, which is provided by a frequency generator outside the magnet room, to generate horizontal vibrations. The alternating flux of the coil interacts with the magnetic field, yielding a cyclic electromagnetic torque that causes the actuator arm to vibrate. One end of the actuator rod is responsible for the conveying of the vibrations into the agarose. Initially, a downward facing rubber ball was conceivable to transfer the vibrations. This rubber ball was later substituted by a flat plate for a better penetration of the shear wave across the entire gel. For a better coupling to the agarose gel/mouse chest, the actuator rod was fixed with a plastic band. The solenoid coil was positioned outside the animal cradle to minimize interference with the magnetic field gradients during the imaging acquisition.

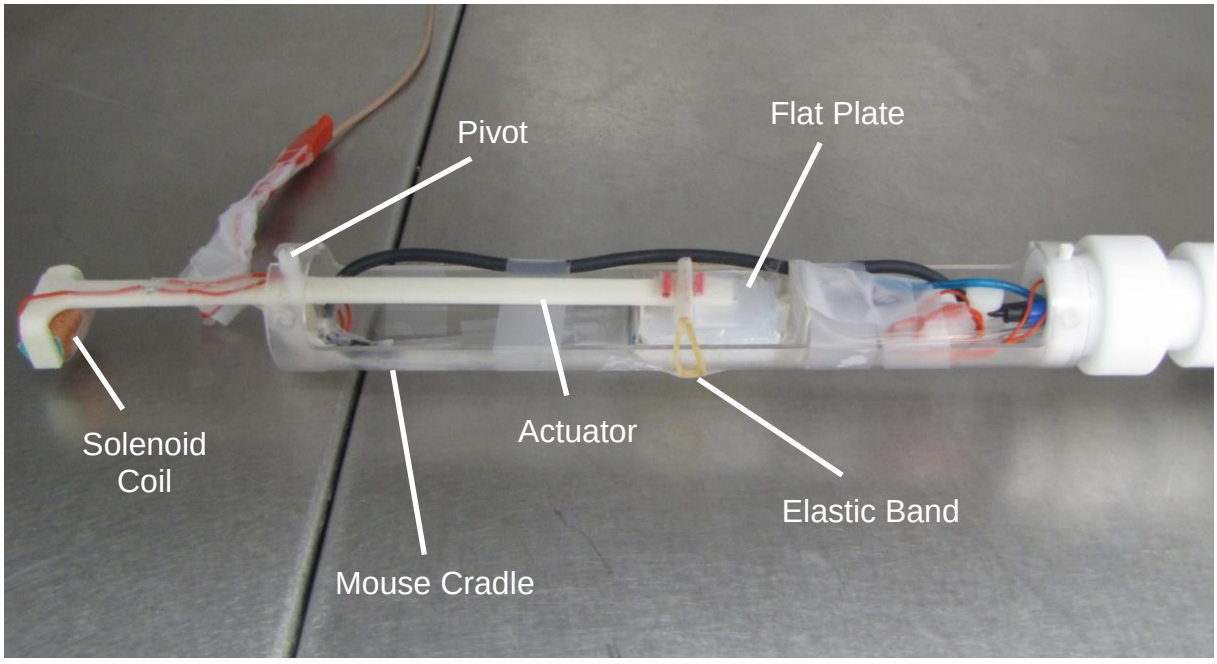

Figure 2.1. Experimental system for generating strain waves in the magnet. The actuator consists of an electrical coil attached to a pivot bar that is driven by a wave generator. The alternating flux of the coil interacts with the main magnetic field of the imager, producing a cyclic force, which is coupled by a contact plate to the surface of the object under investigation.

2.2 Phantom Experiments

To test the hypothesis that the proposed method can be used to quantitatively image the characteristics of propagating mechanical waves, experiments were performed in phantoms made of agarose gels. Phantoms consisting of 0.5% and 1% of agarose gel and spiked with 1mM Gd-DTPA (a paramagnetic contrast agent used to shorten the T_1 relaxation time) were imaged at different frequencies between 500 Hz and 1500 Hz with the motion-sensitizing gradients applied in readout, phase-encoding and slice-selection directions, respectively. Images covering one full cycle of the vibration cycle were acquired in each direction.

The technique was then applied to a two-compartment phantom with two vertical layers of different concentrations of agarose gel. The phantom was made of a soft gel of 0.5% of agarose in one side and a stiff gel with 2% of agarose in the other side (both spiked with 1 mM of Gd-DPTA). Mechanical stimulation was induced at the top of the two-compartment phantom at a vibration frequency of 500 Hz. Shear waves were encoded in phase-encoding direction, which was the direction of external vibration. Data covering six complete vibrations cycles were acquired.

2.3 Mouse Experiments

In order to conduct a proof-of-principle experiment, a dead mouse was imaged. The mouse was placed in the MRE apparatus in the supine position. The flat plate was replaced by a concave plate in order to better adapt to the mouse's chest and to get better wave penetration. Images were acquired at vibration between 500 Hz and 1500 Hz. Motion-encoding gradients were applied in phase-encoding, read-out and slice-selection to encode shear waves in all directions.

2.4 Magnetic Resonance Imaging

Imaging was performed on a horizontal 210 mm bore 9.4 T magnet, VNMRS Direct drive console, comprising a high-performance 1000 mT/m actively shielded gradient system (Agilent Technologies, Yarnton, UK). Experiments were carried out using a 42 mm i.d. actively decoupled quadrature-driven birdcage resonator (Rapid Biomedical, Rimpar, Germany).

MR-sequences were implemented to encode shear deformation. The established phase-contrast cine-MRI sequence used previously to assess myocardial wall motion (Dall'Armellina *et al*., 2012) a gradient-echo MRI sequence was modified to incorporate sinusoidal motion-sensitizing gradients (Figure 2.2) with frequencies up to 1.5 kHz.

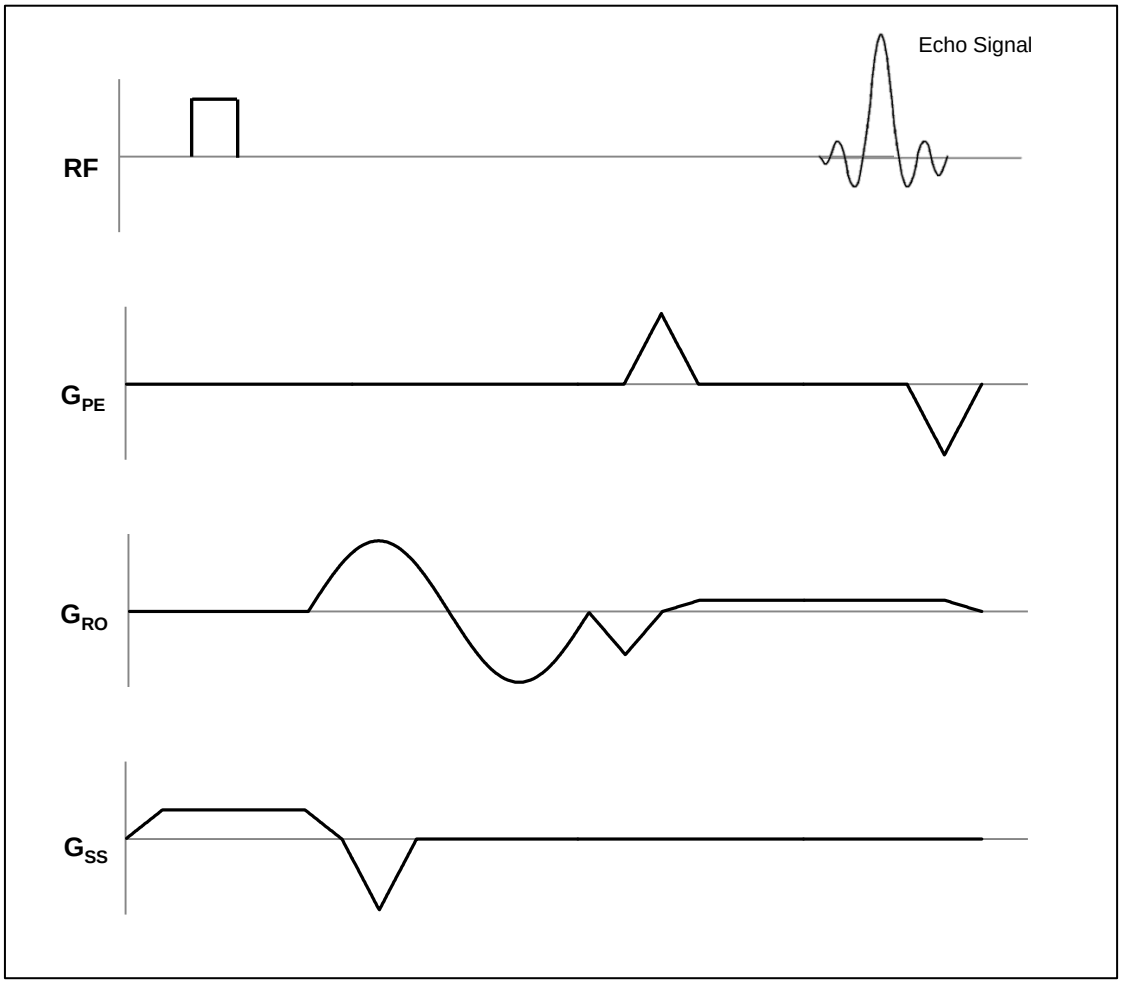

Figure 2.2. MRE pulse sequence schematic diagram. The figure depicts the gradient-echo pulse sequence equipped with a sinusoidal motion-sensitizing gradient in the read-out direction. The motion-sensitizing gradients can also be applied in phase-encoding and slice-selection directions.

Typical acquisition parameters for the single agarose phantom experiments were: TR= 10 ms; TE= 2.08 ms; field of view (FOV) 36x36 mm; motion-sensitizing gradients' strength= 600 mT/m; slice thickness = 1 mm; number of points on the vibration curve = 20. For the two-compartment phantom, the acquisition parameters were: TR= 50 ms; TE= 2.08 ms; FOV 40x40 mm; motion-sensitizing gradients' strength= 600 mT/m; slice thickness = 1 mm; number of points on the vibration curve = 120. For the mouse experiments the acquisition parameters were: TR= 50 ms; TE= 2.08 ms; FOV 36x36 mm; motion-sensitizing gradients' strength= 600 mT/m; slice thickness = 1 mm; number of points on the vibration curve = 120. In all experiments the driving voltage was set 10 Vpp at the signal generator.

All experiments were carried out in a semi-cylindrical plastic mouse cradle of 39 mm.

CHAPTER 3

Results

3.1 Phantom Experiments

The Figure 3.1 shows a magnitude MR image to illustrate the orientation of the MR gradients used in the study. The image also demonstrates the position of the actuator, which corresponds to the origin of the mechanical excitation. The vibrations were applied on top of the phantoms, causing the gels to move in phase-encoding direction.

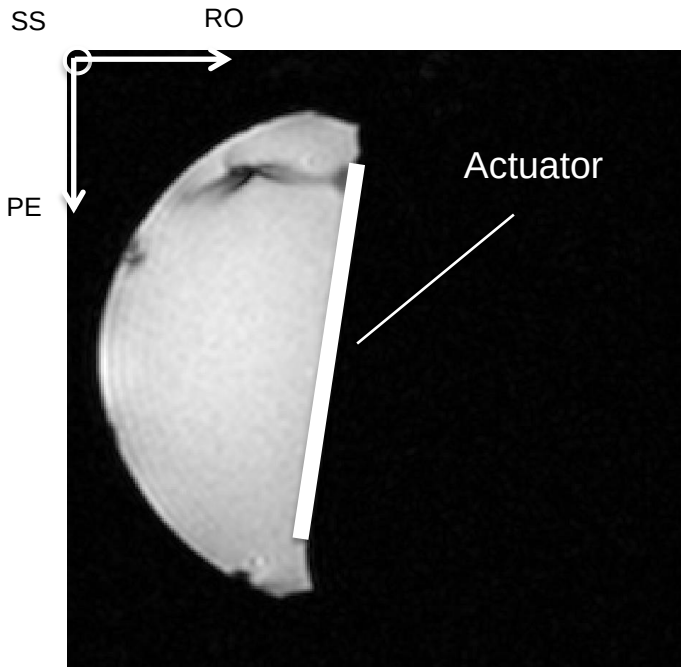

Figure 3.1. Gradient-echo MR image of 0.5% agarose phantom in axial orientation. The picture shows the actuator position and orientation of MR gradients.

Images of shear wave propagation across the 0.5% agarose phantom are presented in Figure 3.2. The figure shows transverse phase images with motion-sensitizing gradient applied in phase-encoding, read-out and slice-selection directions, respectively. Shear wave stimulation was obtained using a vibration frequency of 500 Hz with the mechanical excitation applied in phase-encoding direction.

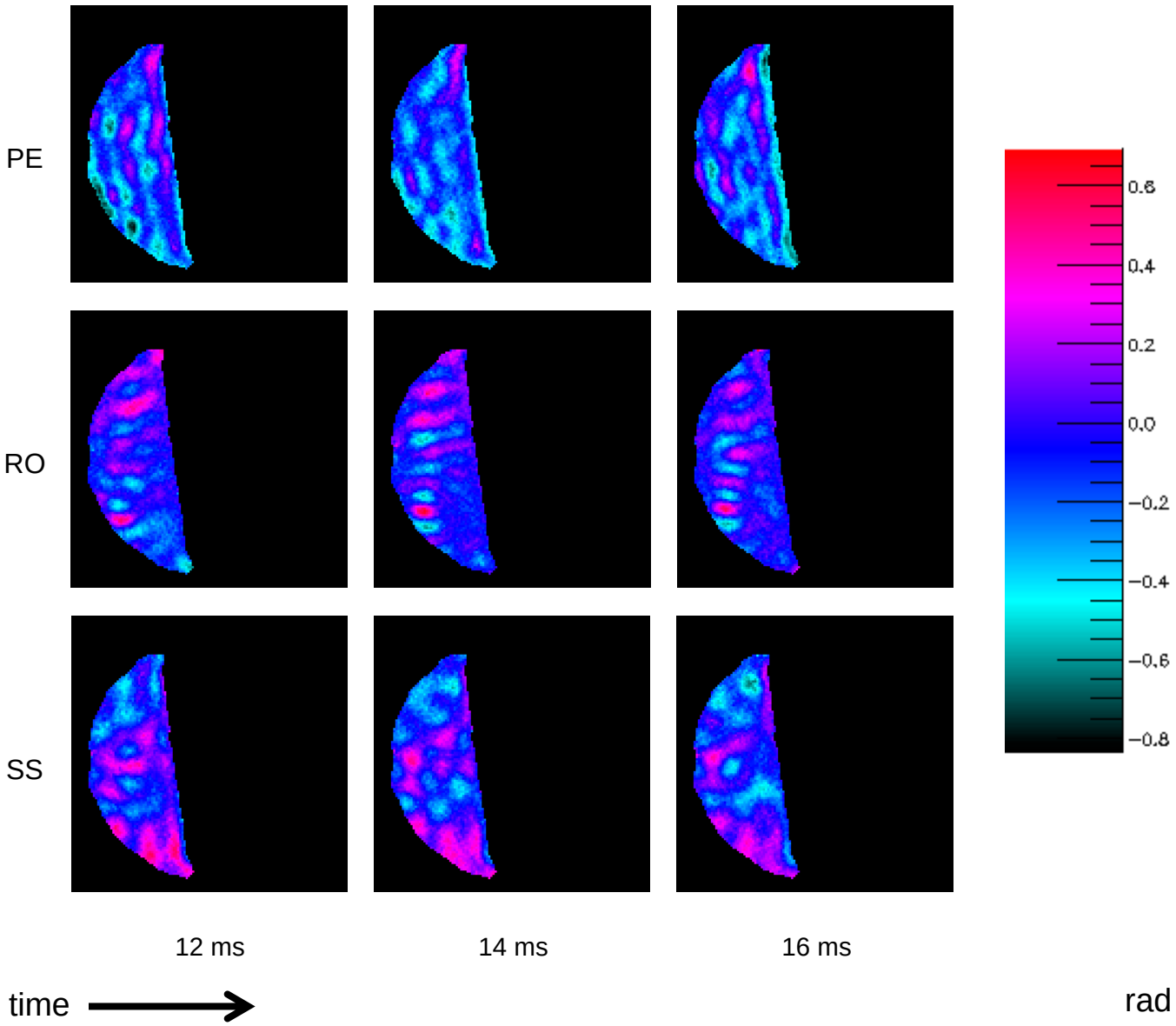

Figure 3.2. Propagating shear waves in agarose phantoms in all directions. The images show shear wave propagation at 0.5% agarose phantom, showing motion in phase-encoding, read-out and slice-selection directions, at 500 Hz. Shear waves can be seen most clearly in phase-encoding direction, which is the direction of excitation.

The color-coded images in Figure 3.2 demonstrate a pattern of phase shifts of the spins. This pattern corresponds to shear wave propagation, which is translated into displacement of the spins about their mean position. Thus, there is a clear uniform penetration of shear waves in phase-encoding direction, which is the direction of mechanical excitation. It is also possible to observe some movement in read-out and slice-selection directions

The plots in Figure 3.3 show the phase changes quantitatively in a selected region of interest (ROI) of the image, close to the actuator, which follows a sinusoidal pattern.

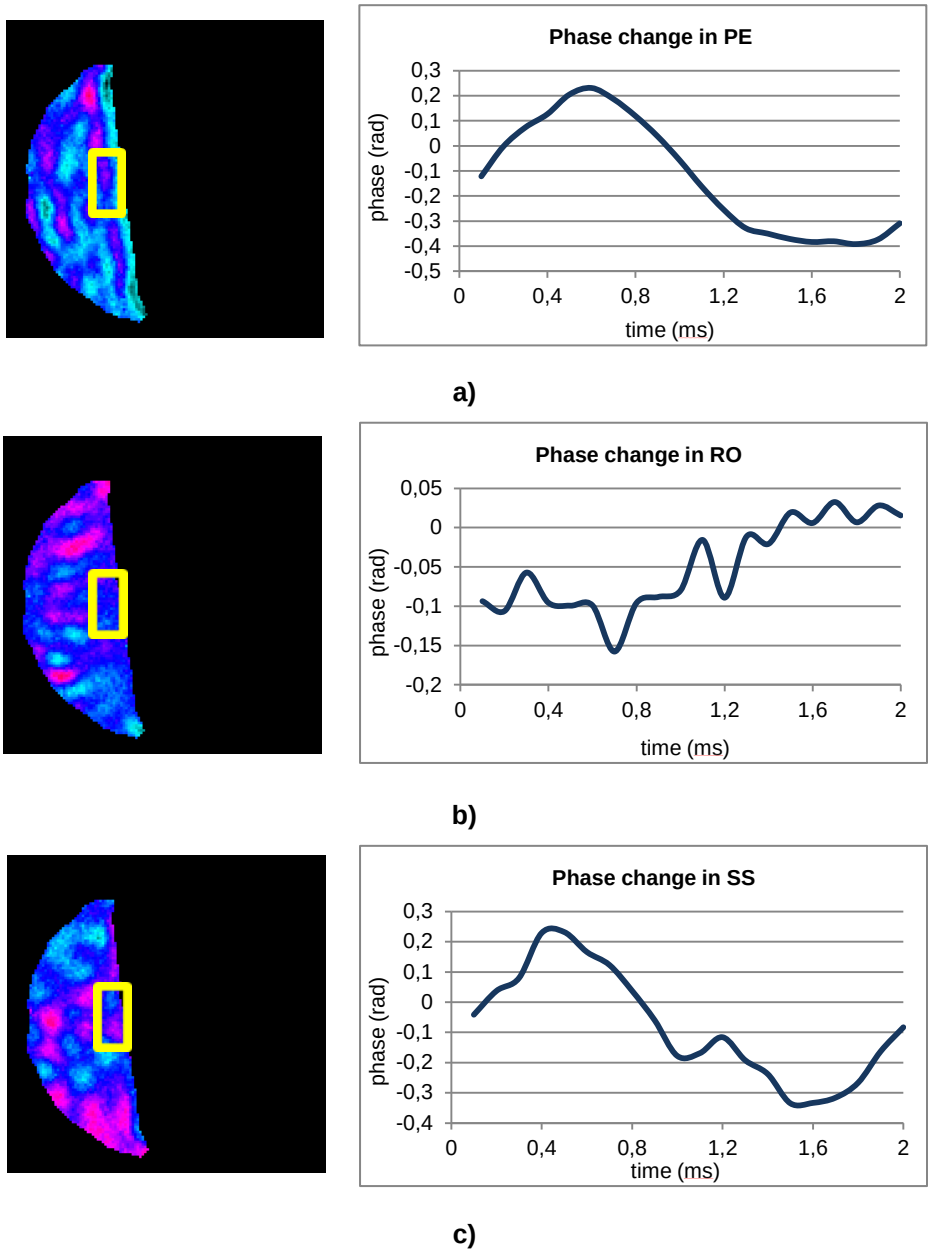

Figure 3.3. Phase change of a 0.5% agarose gel phantom. The plots show a sinusoidal behavior of the spins in **a)** phase-encoding, **b)** read-out and **c)** slice-selection directions. The images were acquired with sixteen time points in a complete vibration cycle at 500 Hz.

In order to better illustrate the elastic and viscous behavior of different materials with distinct mechanical properties, two phantoms with different agarose concentrations were imaged at different frequencies of stimulation. Figure 3.4 shows experiments on 0.5% and 1% agarose gels with shear-wave excitation of 500 Hz and 1000 Hz. These MR images demonstrate planar shear waves propagating down from the surface, which uniformly penetrate the phantom in both cases. Both gels have different mechanical properties which results in a shorter wavelength in the 0.5% gel than the wavelength found in the stiffer gel. According to the color scale, Figure 3.4 also shows higher

attenuation of the shear waves at 1% agarose gel, either at 500 Hz or 1000 Hz, when compared with the propagation of waves in 0.5 %.

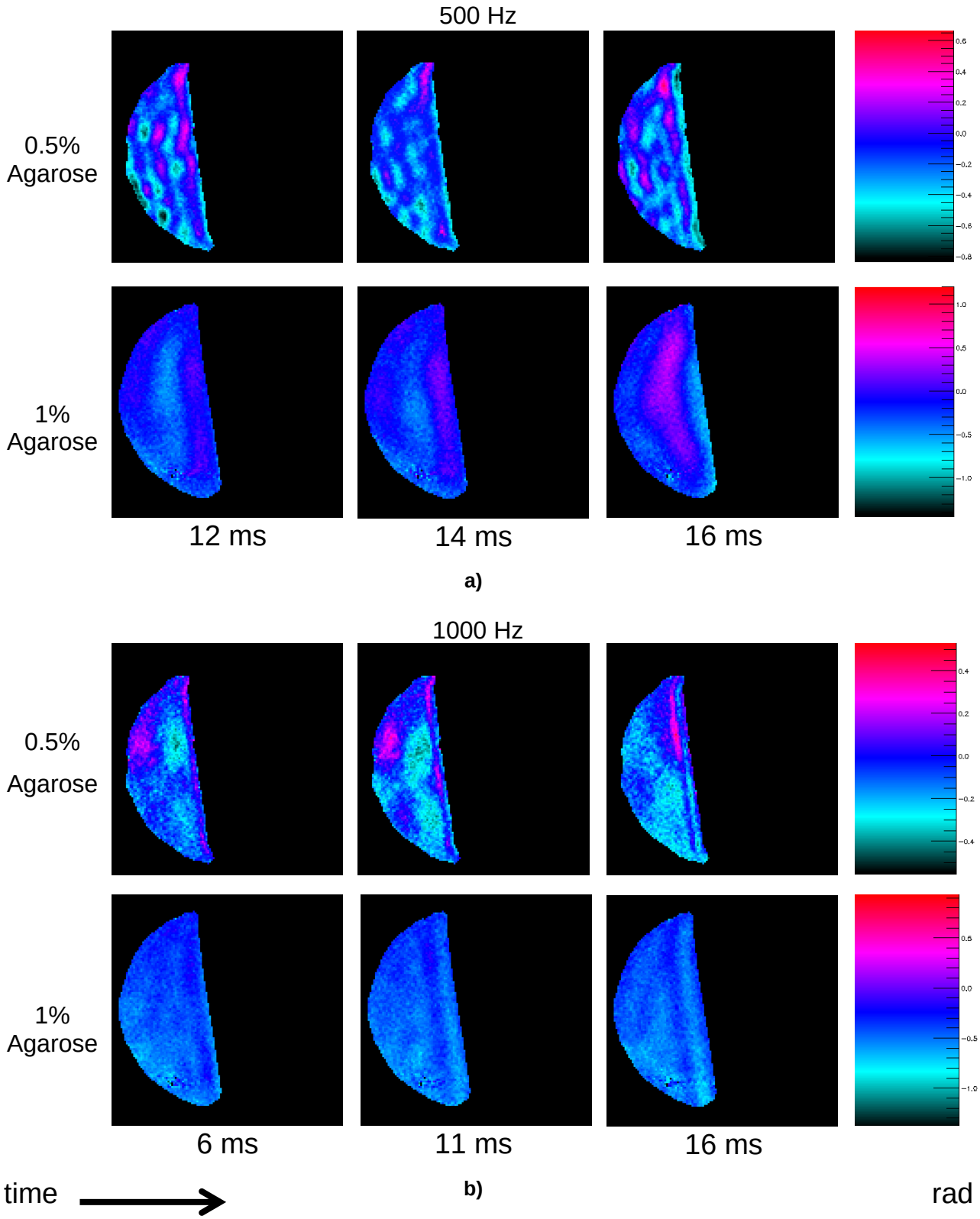

Figure 3.4. Phantom experiment demonstrating the effect of shear wave propagation in two different phantoms with distinct agarose concentrations. Phantoms of 0.5% and 1% agarose were exited **a)** at 500 Hz and **b)** at 1000 Hz.

In order to illustrate wave propagation in a material with different mechanical properties, a two-compartment phantom with different concentrations was imaged (Figure 3.5). The phantom consisted of two vertical layers, with a compartment of 0.5% agarose gel, and another compartment with higher stiffness gel of 2 % agarose. Mechanical stimulation was induced over the top of phantom at a vibration frequency of 500 Hz. Shear waves were encoded in phase-encoding direction, which was the direction of excitation.

Through the Figure 3.6, it is clearly visible that shear waves penetrate non-uniformly the phantom. There is a better propagation of waves in the softer gel (0.5% agarose) than the rigid gel (2% agarose), resulting in a shorter wavelength in the softer than in the rigid one. Analyzing the propagation of waves in the sequence of images, it can be seen that in the stiffer gel the wavelength exceeds the dimension of the phantom. On the other hand, in the softer gel six complete cycles of the wave motion at 500 Hz are observed. Moreover, spins exhibit a larger displacement in the softer gel (as illustrated by the color-coded phase) than in the stiffer gel, indicating that the 0.5% gel has a higher degree of deformation. The image also demonstrates propagating waves arising from the movement of the animal cradle, causing interference of waves within the softer gel.

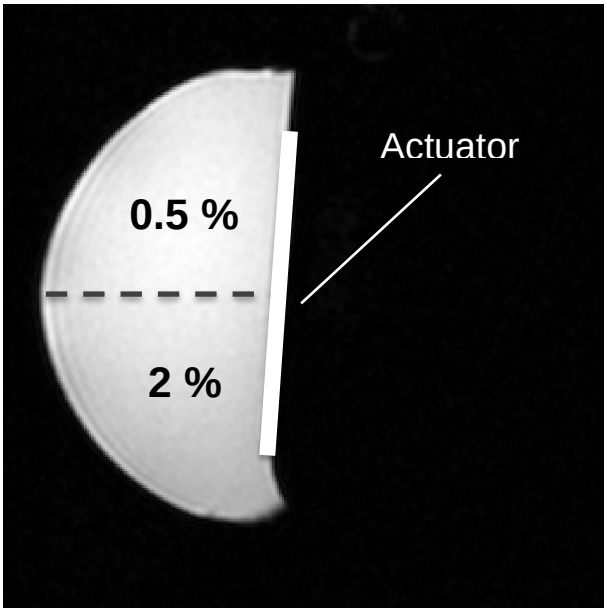

Figure 3.5. Gradient-echo MR image of the two-compartment phantom. The two-compartment gel consisted of 0.5% and 2% of agarose gels. Mechanical stimulation was induced at the top of phantom at a vibration frequency of 500 Hz. Shear waves were encoded in phase-encoding direction, which was the direction of excitation.

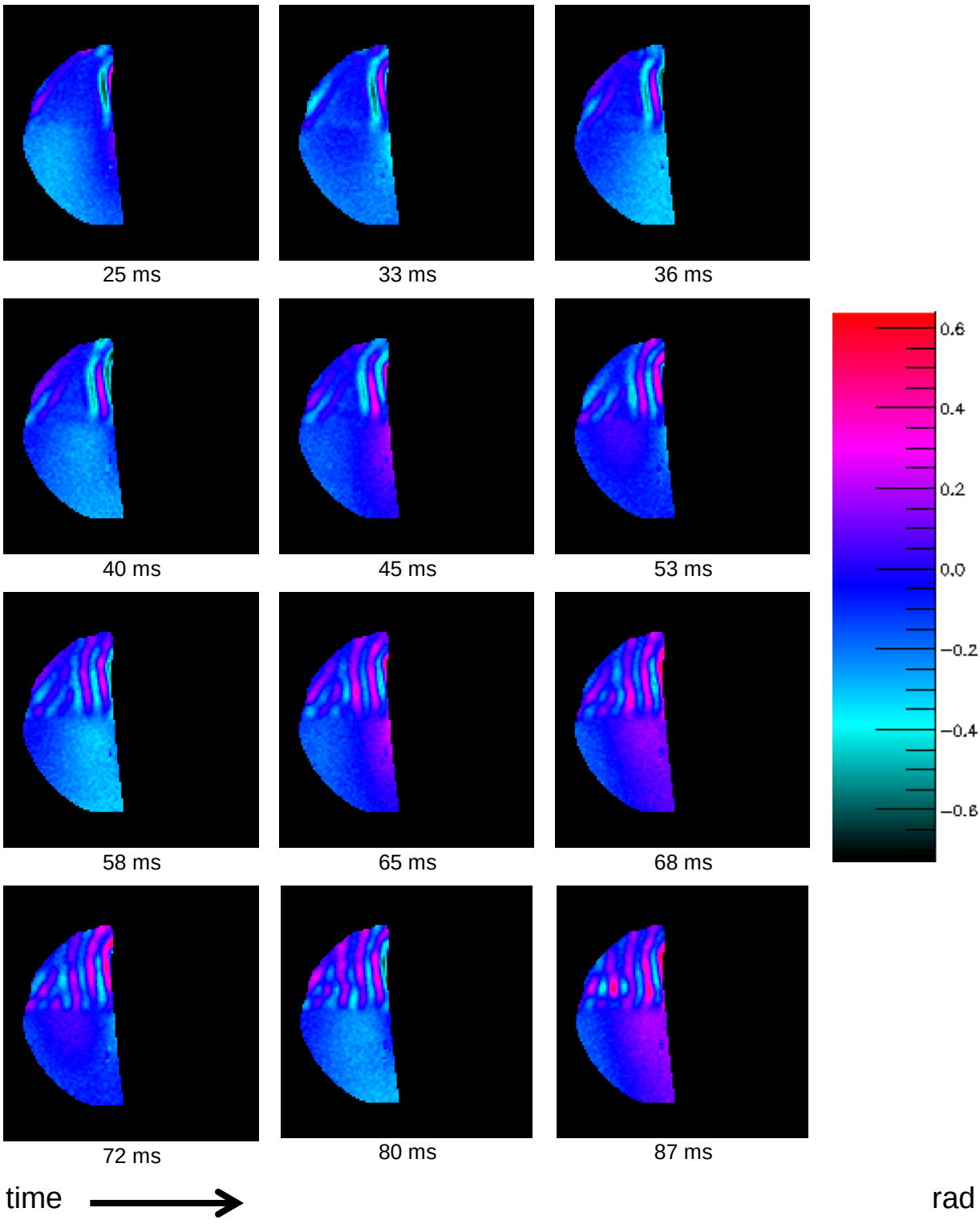

Figure 3.6. Shear wave propagation into a two-compartment phantom varying over time. The upper part refers to the 0.5% gel and the lower part refers to the 2% gel.The resulting displacement image reflects shear wave propagation in a medium of varying stiffness, in phase-encoding direction.

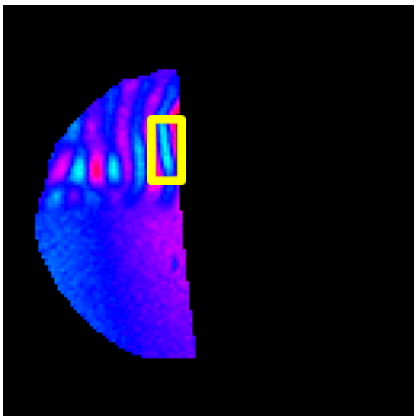

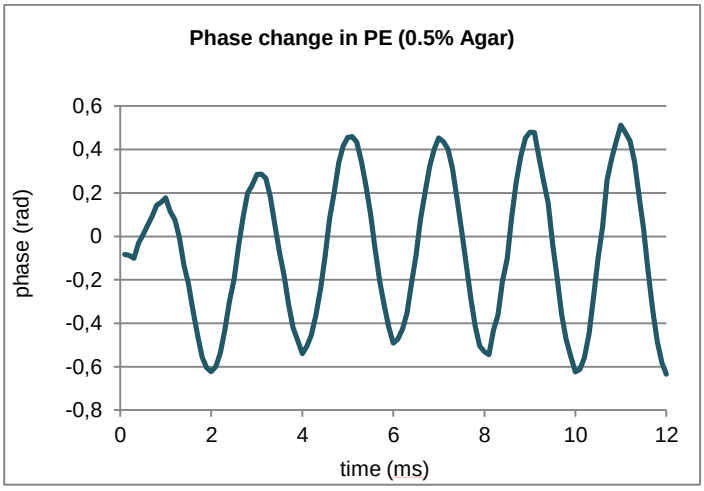

a)

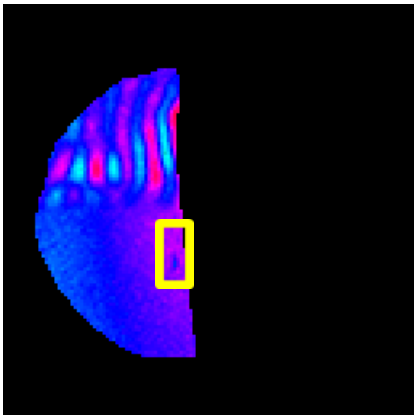

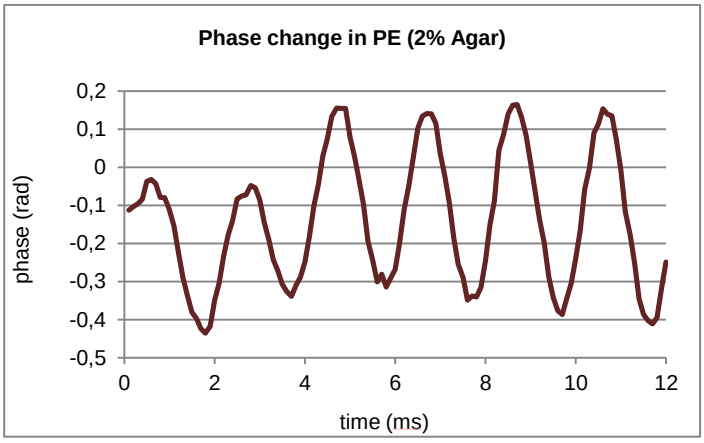

b)

Figure 3.7. Phase change of the two-compartment phantom with **a)** 0.5% and **b)** 2% of agarose gel. The plots show a sinusoidal behavior of the spins in phase-encoding direction, which was the direction of mechanical excitation. The images were acquired with sixteen time points in a complete vibration cycle at 500 Hz.

Figure 3.7 shows a quantitative illustration of the phase evolution. The plots show the phase-shift changes of a ROI, close to the actuator, of each agarose gel compartment. The phase values denoted a sinusoidal pattern indicating the propagation of waves. It is clearly observable that phase-shift variations achieved higher values in the 0.5% agarose gel compartment than in the 2% compartment. These values indicate that these two gels, subjected to the same mechanical stimulation, reacted differently to the excitement. Therefore, according to the phase values shown in Figure 3.7, the 0.5% compartment deformed significantly more than 2% of the compartment.

3.2 Mouse Experiments

Following the experiments on a two-compartment phantom, MR Elastography technique was applied to the tissues of a dead mouse.

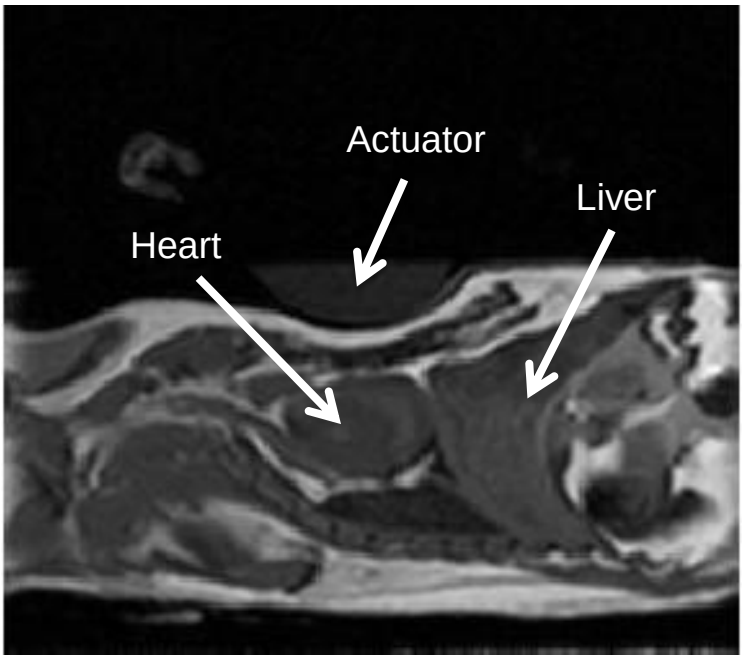

Figure 3.8. 2D anatomical image of the dead mouse in sagittal orientation.

MRE was performed while mechanical excitation was applied to the mouse's chest (Figure 3.9). The frequency of excitation was 100 Hz, with the motion-sensitizing gradient encoding movement in the slice-selection direction. Figure 3.9 clearly shows waves propagating through the mouse body. The phase images show a pattern of phase shifts crossing the different tissues, corresponding to shear wave propagation. Along the passage of the vibrations, mouse organs such as heart, lungs and liver are distinguishable.

The plots in Figure 3.10 show the sinusoidal behaviour of liver and cardiac tissues in response to mechanical vibrations. It is clearly visible that the values of phase evolution vary from the heart to the liver. The liver achieved higher values of phase-shift variations, which means that this tissue deformed significantly more than the heart. These values indicate that these two tissues, subjected to the same mechanical stimulation, reacted differently to the excitement.

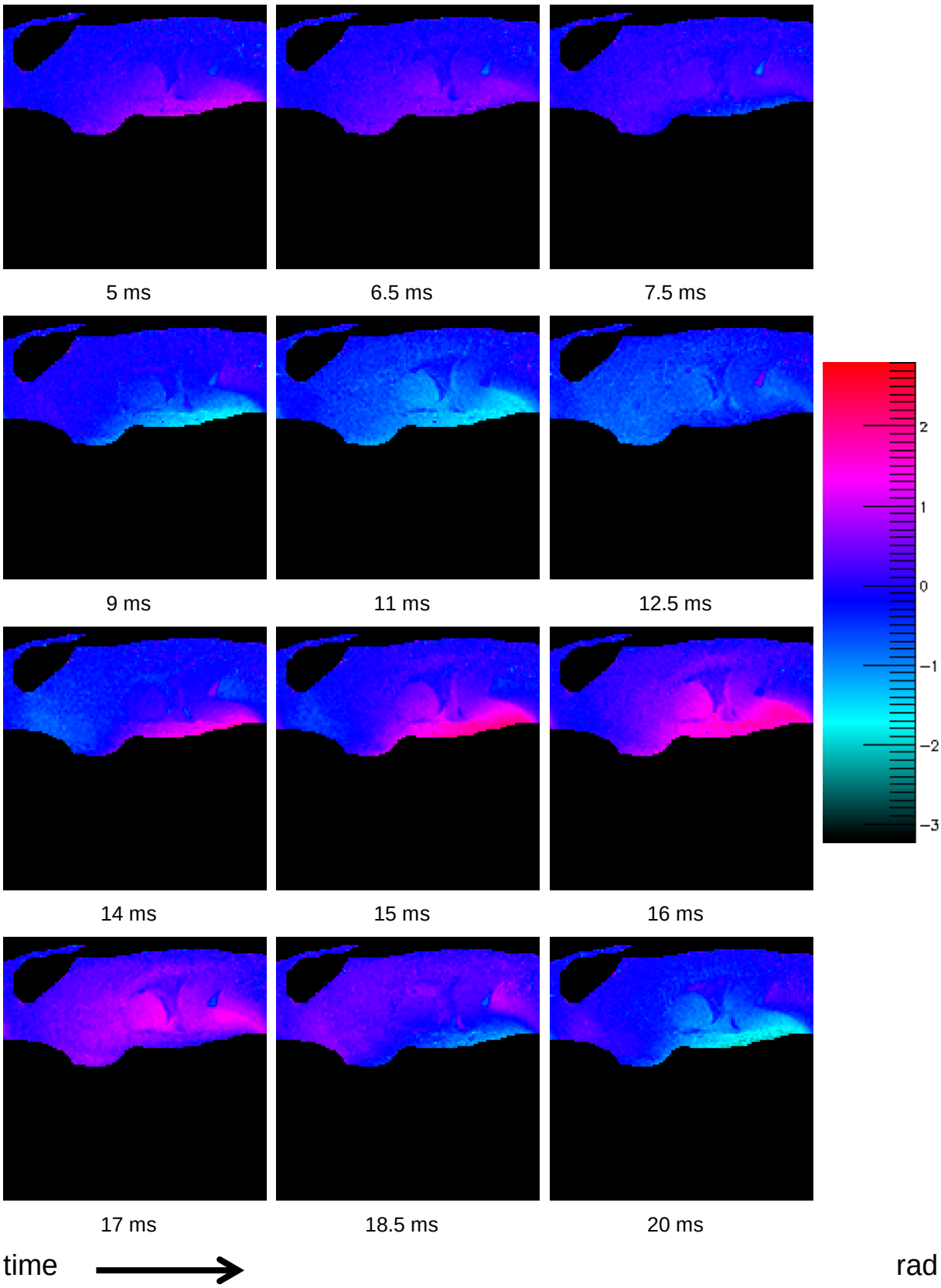

Figure 3.9. Strain waves propagation across the dead mouse. Mechanical stimulation was induced over the top of the dead mouse, at a vibration frequency of 100 Hz. Shear waves were encoded in slice-selection direction.

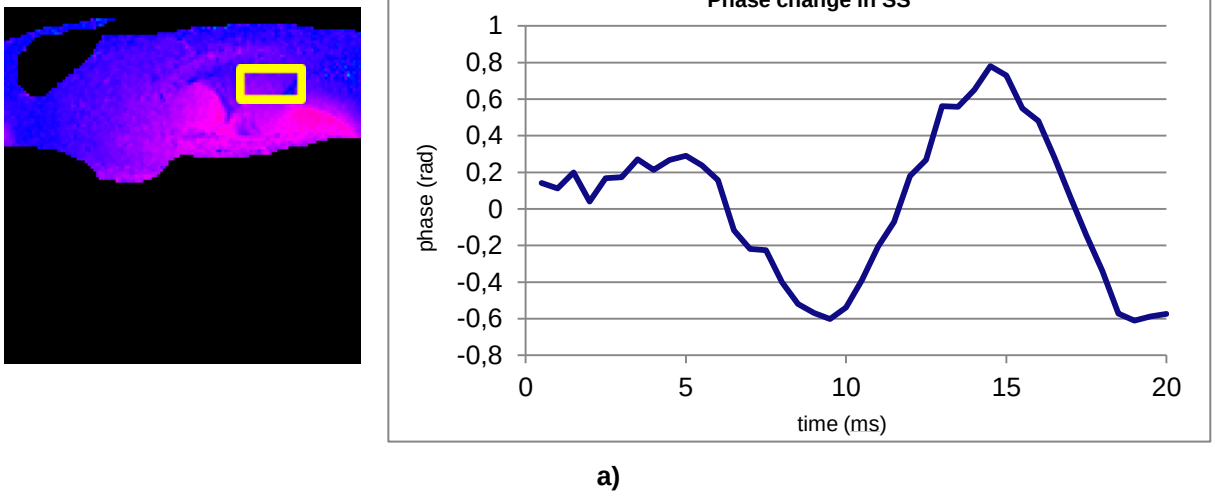

a)

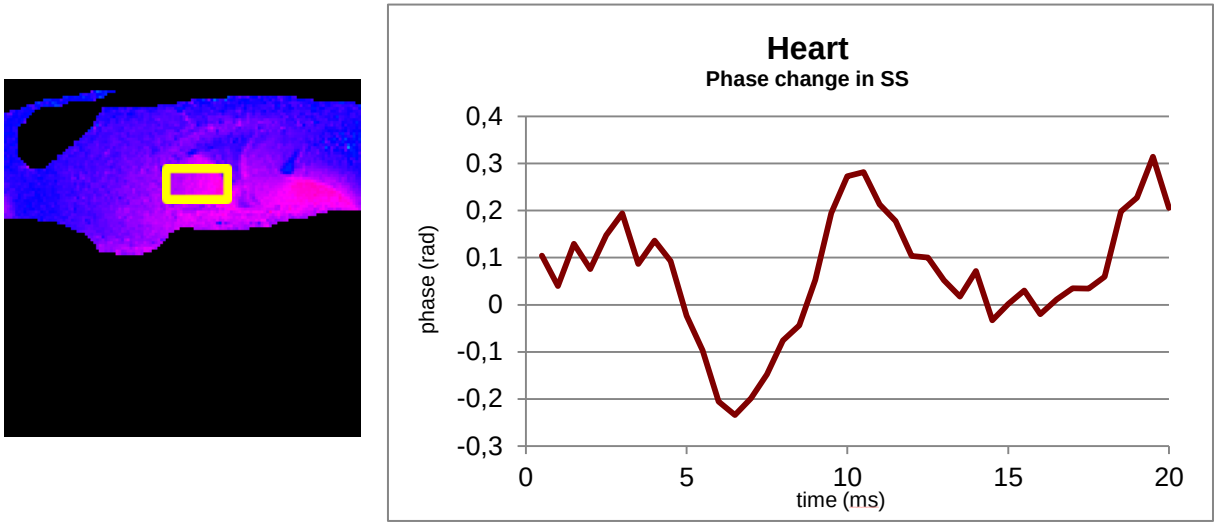

b)

Figure 3.10. Phase change of the mouse **a)** liver and **b)** heart. The plots show a sinusoidal behavior of the spins in slice-selection direction, which was the direction of mechanical excitation. The images were acquired with one- time point in a complete vibration cycle at 100 Hz.

CHAPTER 4

Discussion

Humans share ~ 99% of their genes with mice. Characterization of genetically modified mice gives to researchers information that can be used to better understand how a similar gene may cause or contribute to heart diseases in humans. Specifically, the development of μMRE technique for rodent hearts can play a crucial role for assessing pathologies associated with increased myocardial stiffness such as diastolic dysfunction.

This project represents an important step to develop a non-invasive technique for future LV pressure measurements in mice. In the development of MRE hardware, the design had to specifically overcome the inherent challenges of cardiac MR in rodents at ultra-high magnetic field, such as MR compatibility of the setup and space limitations. Thereby, the design needed to be optimized in order to minimize space requirements without impairing functionality, and to be compatible with the existing animal handling system. The diameter of the used RF-volume coils was 39 mm, so the entire setup was assembled taking into account the available space of both mouse cradle and MR RF coil. As a result, all setup components were designed according to the available space.

Initially, based on the design of Atay *et al.* (2008), the solenoid coil was placed into the mouse's cradle, as close as possible to the vibration end of the actuator rod, to increase the intensity of excitation. Tests of the first MRE setup yielded inconclusive results as it was not possible to unambiguously resolve any vibration transmission. It was found only discontinuities in the phase plots, resulting in a sequence of peaks, instead of a sinusoidal behavior. It was suggested that the MR gradients could be interfering with the MRE setup. Once the solenoid coil moves by the action of a magnetic field, the magnetic fields of MR gradients could be disturbing the coil performance. It was verified from theoretical field plots confidentially provided by Agilent Technology (i.e. the vendor of the MR system) that the solenoid coil was indeed positioned in a hotspot where the gradient field was maximum. The solenoid coil was therefore placed at a location where the intensity of gradients magnetic fields was zero, minimizing any interaction with them. The pivot remained in its place to ensure that there was enough torque to the actuator rod tip over the gel. As the coil was moved from within the cradle to the outside, its size could be increased. As the solenoid coil is a long coil, i.e. with the length greater than its diameter, the number of turns is proportional to the magnetic field strength created by the coil. Therefore, the number of turns was increased to maximize the vibration intensity, according to the available space.

Other improvements were also taken into account in order to obtain better results, namely the rubber ball was replaced by a flat plate. The rubber ball, which was facing downward, caused severe damages to the gel, which may potentially cause injuries to mouse's tissues. In addition, instead of having a localized vibration with a contact area of the approximately 1.5 cm^2, with the flat plate the contact area was increased to 6.25 cm^2, covering almost the whole gel. Consequently, the entire gel

was affected by shear waves. Additionally, the elastic band was also adapted. It was essential that the elastic band allow for rod horizontal movement, and on the other hand ensures good coupling between actuator and gel/tissue. The elastic band was covered with tape to reduce the friction between the rubber band and sample. Lastly, all materials used were chosen taking into account their compatibility with MR.

Agarose phantoms were tested in order to validate both MRE setup and sequence. Agarose gels were used as a means of simulate mechanical properties of mouse tissues. Furthermore, the phantoms were excited over a wide range of vibration frequency. Murine cardiac MRE requires higher frequencies than in humans as a minimum of a half-wavelength is necessary to reliably resolve two areas of differing stiffness (Shah *et al.*, 2004). Thus, to create waves with short wavelengths relative to the heart dimensions, vibrations were excited up to a kHz-range.

As shown in Figure 3.1, a phantom of 0.5% agarose gel was excited at 500 Hz, whereby motion-sensitizing gradient was applied in phase-encoding, read-out and slice-selection directions, so as to encode motion in each direction. As expected, in Figure 3.2 different phases can be seen along the gel which are color coded in the images. This color difference corresponds to gel deformation as a result of the shear wave's passage. It was also possible to verify that the waves are at their greatest intensity at the top of the gel, which corresponds to flat plate, the excitation source. Waves can be seen most clearly in phase-encoding direction as predicted, which was the direction of excitation. However, there is movement towards slice-selection and read-out directions due to the cylinder-shaped vibrating boundaries of the cradle.

Figure 3.3 depicts spins phase-shift along a full vibration cycle. Due to the mechanical vibrations, the gel deformation reflects the sinusoidal behavior of the gel. These results are in accordance with a driving sinusoidal current, which leads to a mechanical penetration of sine waves.

To better illustrate the effect of different mechanical properties, shear wave propagation was measured and compared in two gels with different agarose concentrations. As already published in the literature, stiffer tissues deform less than softer ones upon the application of mechanical stimulation (Muthupillai *et al*. 1995). The gels with 0.5% and 1% were tested over a wide range of frequencies. Figure 3.4 demonstrates the physical response of both gels to a 500 Hz and 1000 Hz vibration frequency. In Figure 3.4 a), when compared both gels at 500 Hz there is an increase in the wavelength of the wave in the stiffer gel. Furthermore, there is a color attenuation in the 1% gel, which means that the spins got less phase and therefore the 1% gel deformed less than the 0.5% gel. The same behavior occurs in Figure 3.4 b) with both gels at 1000 Hz. This indicates that the gel with 1% agarose deforms less than the softer one when applied mechanical stimulation. It should also be noted that there is a clear decrease in wavelength in the 0.5% agarose gel at 500 Hz compared to 1000 Hz. This indicates that again that the higher frequencies will probably be more suitable for the mouse heart dimensions.

In an attempt to better illustrate the wave propagation in a medium with varying stiffness, a two-compartment phantom was made consisting of 0.5% and 2% agarose gels and subjected to external vibrations of 500 Hz (Figure 3.5). In Figure 3.6 an uniform shear wave penetration throughout both compartments can be seen. In the compartment of 0.5% agarose is noticeable six complete

vibration cycles along the gel, whereas in the 2% compartment the wavelength exceeds the dimension of the phantom. As expected and observed in previous phantom experiments, the softer gel is characterized by shorter wavelengths. Conversely, the wavelength in the stiffer gel is larger than the softer gel, as is visible in Figure 3.6. Besides, in the 0.5% compartment there is color attenuation than in the softer gel, indicating less deformation. The image also demonstrates wave propagation arising from the cradle's bottom causing a convergence effect within the softer gel. This fact was most likely caused by the movement of the entire cradle. The results of Figure 3.6 show that certainly the wave propagation is influenced by the stiffness of the tissues, sustaining the applicability of MRE technique.

Figure 3.7 shows clearly a sinusoidal behavior of the selected ROI's in both 0.5% and 2% compartments. The 0.5% compartment presents a greater range of phase-shifts. As expected, this suggests that the softer had a higher degree of deformation than the stiffer gel.

Since this project was at the beginning of a pilot-study and it is not known whether there is any physiologic impact of mechanical stimulation on mice's tissues, the MRE technique was applied to a dead mouse (Figure 3.8). The setup was modified a slightly on the actuator tip. The first attempt in acquiring images did not exhibit any wave propagation in the tissues, necessitating the replacement of this part. The rubber ball presented a localized vibration. Thus, a concave plate was used in order to cover the chest for a better adaptation and to provide better wave penetration, which represented an improvement. The results in Figure 3.9 present shear wave propagation from the chest throughout the body. There is a clear tissue distinction when vibrations pass through them. The tissues deformed depending on their rigidity as indicated by the phase plots. The vibration frequency used in the mouse experiments was 100 Hz. At higher frequencies the vibrations appeared to loose and it was not possible to see any wave propagation trough the mouse's body. As it can be seen in Figure 3.9, significantly higher stimulation frequencies will be required to obtain considerably small wavelengths in order to resolve the cardiac dimensions.

In Figure 3.10, the plots show a sinusoidal behavior of the waves. It is more noticeable in the liver than in the heart, which means that the liver deformed more than the heart. Thus, the heart showed a lower phase variations. The results were only to indicate proof of concept as this was a dead mouse. Various transitions occur in cells, tissues and organs once the organism is dead. It is known that the body undergoes various changes during the time of necrosis in terms of physiology, chemistry, and biology (Su *et al*., 2012). Nevertheless, the results of Figure 3.9 are encouraging as they suggested the MRE technique can distinguish tissues throughout the body by their elasticity.

CHAPTER 5

Conclusions

This was a very auspicious and challenging project. It had various challenges related to the hardware development. The major limitation was space restrictions and the size of the design had to be optimized without impacting the functionality of the MRE setup. However, it was possible to successfully develop a setup and provide mechanical stimulations inside the magnet. In addition, a wide range of frequencies was used covering up to 1.5 kHz, which allowed stimulating from low to high frequencies. Furthermore, it was shown that imaging of shear wave mechanical excitation may be a method to encode properties of a heterogeneous object.

Thus, this project was a significant achievement in the contribution of the ultimate goal, i.e. the ability to develop a technique for indirect LV pressure measurements in mice using MRE.

Hence, the proposed method may add to the portfolio of non-invasive MRI techniques and contribute to a more comprehensive phenotype characterization of rodent models of human heart diseases. Moreover, significant resources are put into the development of realistic computer models of the heart, requiring information on structure, blood-flow, conductivity and function. The ability to validate mechanical properties of normal and disease myocardium will be of significant value, and help to further reduce animal usage on basic scientific research.

CHAPTER 6

Future Research

This pilot study aims to pave the way for non-invasive pressure measurements in mouse hearts. After the success in the development of MRE setup that allows for mechanical stimulation inside the magnet, efficient algorithms will be implemented to extract shear wave amplitude from μMRE data. Afterwards, the plan is to validate the hardware, MRI-sequence and post-processing methods on agarose phantoms. Different-concentration agarose phantoms will be subjected to MRE examinations and will be used to measure the corresponding dynamic shear moduli with shear plate rheometer. After successful validation of these individual agar samples, structured phantoms consisting of 0.5 – 1 mm thick layers with different gel concentrations will be prepared to create more closely the conditions found *in vivo*. The structured phantoms will only be investigated using MRI, and the optimal frequency range will be determined. In this stage, μMRE setup will be fully validated in phantoms and ready for application in mouse hearts. Subsequently, in order to exclude any adverse effect from the mechanical tissue stimulation on cardiac function, will be evaluated the impact of mechanical excitation in mouse hearts with a fully characterized physiological impact of μMRE setup.
In the final stage, and under the premise that no adverse effects from the mechanical vibration will be observable, this technique will be applied to health mouse hearts with variability and reproducibility assessment in which μMRE data will be acquired.

References

Atay, S. M., Kroenke, C. D., Sabet, A., Bayly, P. V. 2008. Measurement of the Dynamic Shear Modulus of Mouse Brain Tissue *In Vivo* By Magnetic Resonance Elastography. *Journal of Biomechanical Engineering* **130**(2): 021013.

Boulant, N. 2009. **T**1 and **T**2 Effects During Radio-Frequency Pulses in Spoiled Gradient Echo Sequences. *Journal of Magnetic Resonance* **197**: 213–218.

Bydder, G. M., Hajnal, J. V., Young, I. R. 1998. MRI: Use of the Inversion Recovery Pulse Sequence. *Clinical Radiology* **53**: 159–176.

Dall'Armellina, E., Jung B. A., Lygate C. A., Neubauer, S., Markl, M., Schneider, J. E., 2012. Improved Method for Quantification of Regional Cardiac Function in Mice using Phase-Contrast MRI. *Magnetic Resonance in Medicine* **67**(2): 541–551.

Elgeti, T., Beling, M., Hamm, B., Braun, J., Sack, I. 2010a. Elasticity-based Determination of Isovolumetric Phases in the Human Heart. *Journal of Cardiovascular Magnetic Resonance* **12**: 60.

Elgeti, T., Beling, M., Hamm, B., Braun, J., Sack, I. 2010b. Cardiac Magnetic Resonance Elastography: Toward the Diagnosis of Abnormal Myocardial Relaxation. *Investigative Radiology* **45**(12): 782–787.

Elgeti, T., Laule, M., Kaufels, N., Schnorr, J., Hamm, B., Samani, A., Braun, J., Sack, I. 2009. Cardiac MR Elastography: Comparison With Left Ventricular Pressure Measurement. *Journal of Cardiovascular Magnetic Resonance* **11**: 44.

Elgeti, T., Rump, J., Hamhaber, U. Papazoglou, S., Hamm, B., Braun, J., Sack, I. 2008. Cardiac Magnetic Resonance Elastography Initial Results. *Investigative Radiology* **43**(11): 762–772.

Elgeti, T., Tzschatzsch, H., Hirsch, S., Krefting, D., Klatt, D., Niendorf, T., Braun, J., Sack, I. 2012. Vibration-Synchronized Magnetic Resonance Imaging for the Detection of Myocardial Elasticity Changes. *Magnetic Resonance in Medicine* **67**: 919–924.

Field, L. J. 1993. Trangenic Mice in Cardiovascular research. *Annual Review of Physiology* **55**: 97–114.

Fullerton, G. D. 1982. Basic Concepts For Nuclear Magnetic Resonance Imaging. *Magnetic Resonance Imaging* **1**: 39–55.

Gadian, D. G. 1995. NMR and Its Applications to Living Systems, 2nd edition. Oxford University Press Inc., New York, pp. 283.

General Electric Company. s.d. NMR – A Perspective on Imaging. General Electric. pp. 4-27.

Glaser, K. J., Manduca, A., Ehman, R. L. 2012. Review of MR Elastography Applications and Recent Developments. *Journal of Magnetic Resonance Imaging* **36**: 757–774.

Gore, J. C., Pope, C. F., Sostman H. D. 1986. Errors in the Assessment of the Efficacy of MRI Pulses Sequences. *Magnetic Resonance Imaging* **4**: 251–255.

Graaf., R. A. 2007. In Vivo NMR Spectroscopy Principles and Techniques, 2nd edition. Wiley-Interscience, 592.

Graves, M. J. 2007. Pulse Sequences for Contrast-Enhanced Magnetic Resonance Imaging. *Radiography* **13**: e20–e30.

Haase, A., Jakob, P. M. 1998. Basic Pulse Sequences for Fast Cardiac MR Imaging. *Magnetic Resonance Materials in Physics, Biology and Medicine* **6**: 84–87.

Hendrick, R. E., Nelson, T. R., Hendee, W. R. 1984. Optimizing Tissue Contrast in Magnetic Resonance Imaging. *Magnetic Resonance Imaging* **2**: 193–204.

Jung, B., Markl, M., Foll, M., Hennig, J. 2006. Investigating Myocardial Motion by MRI Using Tissue Phase Mapping. *European Journal of Cardio-thoracic Surgery* **29S:** S150–S157.

Karamitsos, T., Neubauer, S., Cardiovascular Magnetic Resonance Imaging. *Medicine* **38**: 7.

Karstaedt, N., Dixon, R. L., Wolfman, N. T., Ekstrand, K. E. 1983. Nuclear Magnetic Resonance Imaging. *Surgical Neurology* **19**: 206–214.

Klatt, D., Asbach, P., Rump, J., Papazoglou, S., Somasundaram, R., Modrow, J., Braun, J., Sack, I. 2006. *In Vivo* Determination of Hepatic Stiffness Using Steady-State Free Precession Magnetic Resonance Elastography. *Investigative Radiology* **41**(12): 841–848.

Kolipaka, A., Araoz, P. A., McGee, K. P., Manduca, A., Ehman, R. L. 2010. Magnetic Resonance Elastography as a Method for the Assessment of Effective Myocardial Stiffness Throughout the Cardiac Cycle. *Magnetic Resonance in Medicine* **64**(3): 862–870.

Manduca, A., Lake, D. S., Kruse, S. A., Ehman, R. L. 2003. Spatio-Temporal Directional Filtering for

Improved Inversion of MR Elastography Images. *Medical Image Analysis* **7**(4): 465–473.

Manduca, A., Oliphant, T. E., Dresner, M. A., Mahowald, J. L., Kruse, S. A., Amromin, E., Felmlee, J. P., Greenleaf, J. F., Ehman, R. L. 2001. Magnetic Resonance Elastography: Non-Invasive Mapping of Tissue Elasticity. *Medical Image Analysis* **5**: 237–254.

Mariappan, Y. K., Glaser, K. J., Ehman, R. L. 2010. Magnetic Resonance Elastography: A Review. *Clinical Anatomy* **23**(5): 497–511.

Muthupillai, R., Lomas, D. J., Rossman, P. J., Greenleaf, J. F., Manduca, A., Ehman, R. L. 1995. Magnetic Resonance Elastography by Direct Visualization of Propagating Acoustic Strain Waves. *Science* **269**(5232): 1854–1857.

Muthupillai, R., Rossman, P. J., Lomas, D. J., Greenleaf, J. F., Riederer, S. J., Ehman, R. L. 1996. Magnetic Resonance Imaging of Transverse Acoustic Strain Waves. *Magnetic Resonance in Medicine* **36**(2): 266–274.

Myerson, S. G., Holloway, C. J., Francis, J. M., Neubauer, S. 2011. Cardiovascular Magnetic Resonance (CMR) – an Update and Review. *Progress in Nuclear Magnetic Resonance Spectroscopy* **59**: 213–222.

Ophir, J., Cespedes, I., Ponnekanti, H., Yazdi, Y., Li, X. 1991. Elastography: A Quantitative Method for Imaging the Elasticity of Biological Tissues. *Ultrasonic Imaging* **13**: 111–134.

Parker, K. J., Huang, S. R., Musulin, R. A., Lerner, R. M. 1990. Tissue Response to Mechanical Vibrations for “Sonoelasticity Imaging”. *Ultrasound in Medicine & Biology* **16**(3): 241–246.

Ruff, J., Wiesmann, F., Hiller, K., Voll, S., Kienlin, M., Bauer, W. R., Rommel, E., Neubauer, S., Haase, A. 1998. Magnetic Resonance Microimaging for Noninvasive Quantification of Myocardial Function and Mass in the Mouse. *Magnetic Resonance in Medicine* **40**: 43–48

Sack, I., Rump, J., Elgeti, T., Samani, A., Braun, J. 2009. MR Elastography of the Human Heart: Noninvasive Assessment of Myocardial Elasticity Changes by Shear Wave Amplitude Variations. *Magnetic Resonance in Medicine* **61**: 668–677.

Salameh, N., Larrat, B., Abarca-Quinones, J., Pallu, S., Dorvillius, M., Leclercq, M., Leclercq, I., Fink, M., Sinkus, R., Beers, B. 2009. Early Detection of Steatohepatitis in Fatty Rat Liver by Using MR Elastography**.** *Radiology* **253**(1): 90–97.

Schneider, J. E., Cassidy, P. J., Lygate, C., Tyler D. J., Wiesmann, F., Grieve, S. M., Hulbert, K.,

Clarke, K., Neubauer, S. 2003. Fast, High-Resolution In Vivo Cine Magnetic Resonance Imaging in Normal and Failing Mouse Hearts on a Vertical 11.7 T System. *Journal of Magnetic Resonance Imaging* **18**(6): 691–701.

Schneider, J. E., Stork, L., Bell, J. T., Hove, M., Isbrandt, D., Clarke, K., Watkins, H., Lygate, C. A., Neubauer, S. 2008. Cardiac Structure and Function During Ageing in Energetically Compromised Guanidinoacetate N-Methyltransferase (GAMT) - Knockout Mice – a one Year Longitudinal MRI Study. *Journal of Cardiovascular Magnetic Resonance* **10**(1): 9.

Shah, N. S., Kruse, S. A., Lager, D. J., Farell-Baril, G., Lieske, J. C., King, B. F., Ehman, R. L. 2004. Evaluation of Renal Parenchymal Disease in a Rat Model With Magnetic Resonance Elastography. *Magnetic Resonance in Medicine* **52**(1): 56–64.

Srinivasan, S., Krouskop, T., Ophir, J. 2004. A Quantitative Comparison of Modulus Images Obtained Using Nanoidentation With Strain Elastograms. *Ultrasound in Medicine & Biology* **30**(7): 899–918.

Su, R., Ermilov, S., Liopo, A., Oraevsky, A. 2012. Optoacoustic 3D Visualization of Changes in Physiological Properties of Mouse Tissues from Live to Postmortem. *Photons Plus Ultrasound: Imaging and Sensing.* **8223:** 82230K–3.

Techavipoo, U., Chen, Q., Varghese, T., Zagzebski, J. A. 2004. Estimation of Displacement Vectors and Strain Tensors in Elastography Using Angular Insonifications. *IEEE Transactions on Medical Imaging* **23**(12): 1479–1489.

Tzschatzsch, H., Elgeti, T., Retting, K., Kargel, R., Klaua, R., Schultz, M., Braun, J., Sack, I. 2012. *In Vivo* Time Harmonic Elastography of the Human Heart. *Ultrasound in Medicine & Biology* **38**(2): 214–222.

Wuerfel, J., Paul, F., Beierbach, B., Hamhaber, U., Klatt, D., Papazoglou, S., Zipp, F., Martus, P., Braun, J., Sack, I. 2010. MR-Elastography Reveals Degradation of Tissue Integrity in Multiple Sclerosis. *NeuroImage* **49**: 2520–2525.

Xu, L., Chen, J., Yin, M., Glaser, K. J., Chen, Q., Woodrum, D. A., Ehman, R. L. 2012. Assessment of Stiffness Changes in the *Ex Vivo* Porcine Aortic Wall Using Magnetic Resonance Elastography. *Magnetic Resonance Imaging* **30**: 122–127.

APPENDIX

Appendix I

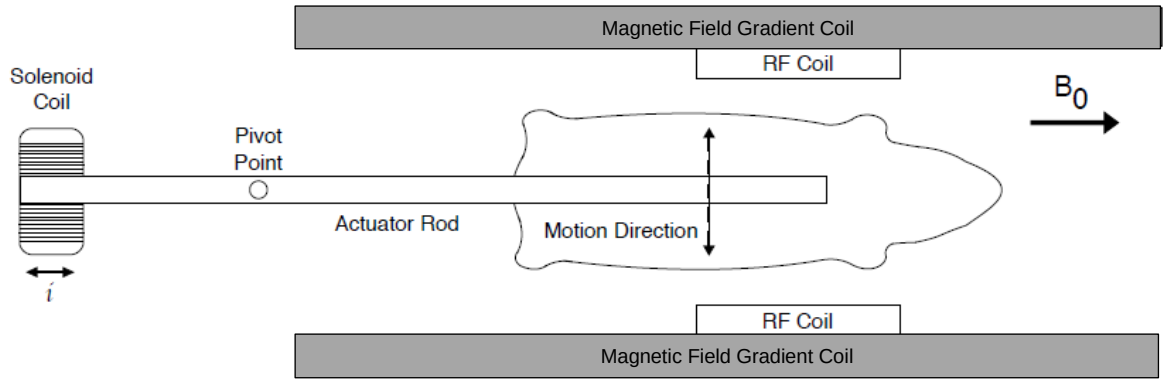

a)

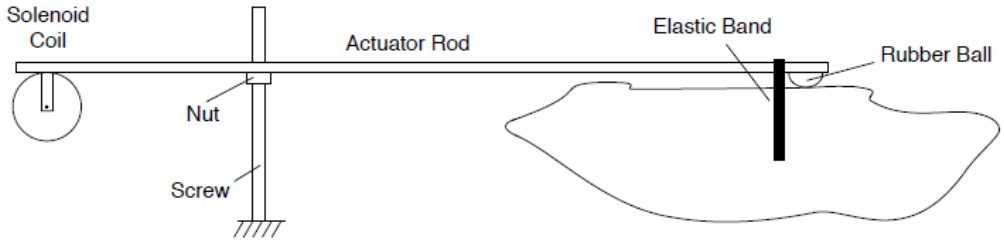

b)

Figure A1. Schematic diagram of mechanical setup based on the design by Atay *et al.* (2008). **a)** Top view of the wave-generating actuator. A small solenoid coil is placed perpendicular to the static magnetic field B_0 and drives a sinusoidal current "i". An electromagnetic torque is developed causing the rod to vibrate horizontally. **b)** A side view of the apparatus showing one end of the actuator that is fitted with a rubber ball and fixed on the chest of the mouse (positioned in the supine position in the animal cradle), while the other actuator end is able to pivot the mechanism.